

# Correlation and Initial Orbit Determination for Short-Arc Optical Observations

Kohei Fujimoto

Daniel J. Scheeres

*Dept. of Aerospace Engineering Sciences, University of Colorado at Boulder*

## CONFERENCE PAPER

Situational awareness of Earth-orbiting particles is highly important for future human activities in space. For optical observations of debris, multiple observations must be combined in order to determine the orbit of the observed object. It is generally uncertain, however, whether two arbitrary tracks are of the same object, and solving this problem can be computationally intensive. In this paper, we propose a technique of correlating multiple optical observations by means of probability distributions in Poincaré orbit element space.

## 1. INTRODUCTION

Situational awareness of Earth-orbiting particles such as active satellites and space debris is highly important for future human activities in space. Presently, over 300,000 particles have been estimated to exist, and over 80,000 observations are made per day [5]. Observations are made either by radar or optical sensors. For optical observations, which are usually made for objects in medium Earth orbit (MEO) and geostationary orbit (GEO), only the angles and angular rates of the track can be determined. That is, the range and range-rate remain largely unknown. Therefore, in order to determine the orbit of the observed object, multiple observations must be combined. It is generally uncertain, however, whether two arbitrary tracks are of the same object, and solving this problem can be computationally intensive. This is the crux of the *too short arc* (TSA) problem. Milani et al. have proposed a solution for heliocentric orbits where each track is expressed in a 4-dimensional quantity called the *attributable vector*, and by placing a few physical constraints, they restrict the range and range-rate to a region called the *admissible region* [4]. Discretized points on the admissible region are referred to as *Virtual Debris* (VD) *particles*. Tommei et al. expanded this method to Earth orbiting objects [6]. Maruskin et al. introduced another method that uses maps of the admissible region in Delaunay orbit element space [3].

In this paper, we propose a technique of correlating multiple optical observations by means of probability distributions in Poincaré orbit element space. We first define the admissible region mathematically, as well as introduce other necessary concepts (Section 2). We then explain our method and how we incorporate observation data (Section 3). An admissible region for an observation is mapped to the 6-D Poincaré space, which is discretized into many hypercubes or *bins*. At each bin, the density of VD's is determined, and its distribution over the Poincaré space can be regarded as a probability density function (pdf) as to where the observed object may exist. We combine pdf's from multiple observations using Bayes' theorem. A significant computational bottleneck in this proposed method arises from the very large number of VD's that must be mapped non-linearly in order to completely represent the admissible region in 6-D space. We avoid this problem by approximating the admissible region as a conglomerate of smaller subsets, and linearly mapping these regions. Finally, we discuss a MATLAB implementation of our method (Section 4). We simulated correlating 996 error-free optical observations for 8 objects in MEO and GEO over the course of approximately 24 hours. All observations were correctly correlated with no false positives. Even in the presence of observation error, Monte Carlo-like test results suggest that the method will perform well. We also tested the code in more difficult observation geometries to ascertain its limits (Section 5). Namely, we considered the case where 2 objects lie within a discretization unit, where 1 object is observed simultaneously at 2 observatories, and where a satellite constellation is observed at 1 observatory.

## 2. BACKGROUND

In this section, we introduce the mathematical definition of the attributable vector and the admissible region, and both the exact (non-linear) and linearized transformations from topocentric spherical coordinates to Poincaré orbit elements. We also discuss the topology of admissible regions, which are 2-dimensional manifolds embedded in 6-dimensional state space. Unless otherwise stated, all length units in this paper are in Earth radii  $r_E$ , time units in hours, mass units in kilograms, and angles in radians.

Report Documentation Page				Form Approved OMB No. 0704-0188	
Public reporting burden for the collection of information is estimated to average 1 hour per response, including the time for reviewing instructions, searching existing data sources, gathering and maintaining the data needed, and completing and reviewing the collection of information. Send comments regarding this burden estimate or any other aspect of this collection of information, including suggestions for reducing this burden, to Washington Headquarters Services, Directorate for Information Operations and Reports, 1215 Jefferson Davis Highway, Suite 1204, Arlington VA 22202-4302. Respondents should be aware that notwithstanding any other provision of law, no person shall be subject to a penalty for failing to comply with a collection of information if it does not display a currently valid OMB control number.					
1. REPORT DATE <b>SEP 2010</b>		2. REPORT TYPE		3. DATES COVERED <b>00-00-2010 to 00-00-2010</b>	
4. TITLE AND SUBTITLE <b>Correlation and Initial Orbit Determination for Short-Arc Optical Observations</b>				5a. CONTRACT NUMBER	
				5b. GRANT NUMBER	
				5c. PROGRAM ELEMENT NUMBER	
6. AUTHOR(S)				5d. PROJECT NUMBER	
				5e. TASK NUMBER	
				5f. WORK UNIT NUMBER	
7. PERFORMING ORGANIZATION NAME(S) AND ADDRESS(ES) <b>University of Colorado at Boulder, Dept. of Aerospace Engineering Sciences, Boulder, CO, 80309</b>				8. PERFORMING ORGANIZATION REPORT NUMBER	
9. SPONSORING/MONITORING AGENCY NAME(S) AND ADDRESS(ES)				10. SPONSOR/MONITOR'S ACRONYM(S)	
				11. SPONSOR/MONITOR'S REPORT NUMBER(S)	
12. DISTRIBUTION/AVAILABILITY STATEMENT <b>Approved for public release; distribution unlimited</b>					
13. SUPPLEMENTARY NOTES <b>2010 Advanced Maui Optical and Space Surveillance Technologies Conference, 14-17 Sep, Maui, HI. Sponsored in part by AFRL. U.S. Government or Federal Rights License</b>					
14. ABSTRACT					
15. SUBJECT TERMS					
16. SECURITY CLASSIFICATION OF:			17. LIMITATION OF ABSTRACT <b>Same as Report (SAR)</b>	18. NUMBER OF PAGES <b>10</b>	19a. NAME OF RESPONSIBLE PERSON
a. REPORT <b>unclassified</b>	b. ABSTRACT <b>unclassified</b>	c. THIS PAGE <b>unclassified</b>			

## 2.1 The Attributable Vector

For optical-only observations, which are usually made for objects in medium Earth orbit (MEO) and geostationary orbit (GEO), only the angles and angular rates of the track can be determined [3]. That is, the range and range rate remains largely unconstrained, except for a few physical restrictions which can be used to constrain their values. Thus, each track can be mathematically expressed in terms of an *attributable vector*  $\mathcal{A}$  at epoch  $t$  of the observation [6]:

$$\mathcal{A} = (\alpha, \delta, \dot{\alpha}, \dot{\delta}) \in [-\pi, \pi) \times (-\pi/2, \pi/2) \times \mathbb{R}^2, \quad (1)$$

where  $\alpha$  and  $\delta$  specify the topocentric angular position of the debris particle. A discussion of how one may estimate an attributable vector from a given track of data can be found in Maruskin, et al [3]. We use J2000 as our coordinate system so that  $\alpha$  is the right ascension and  $\delta$  is the declination. In addition, information regarding time and the location of the observer should be stored for a more complete description of the track, leading to an extended set  $\mathfrak{X}$ :

$$\mathfrak{X} = (\mathcal{A}, t_0, h, \phi, \Theta) \quad (2)$$

where  $t_0$  is the time of the observation,  $h$  is the altitude of location of observation, and  $\Theta$  and  $\phi$  are the angular position of observation for a geocentric spherical coordinate system. We chose a coordinate system such that  $\Theta$  is the latitude and  $\phi$  is the longitude of the observation point. In the following discussion, we will ignore  $h$ .

## 2.2 The Admissible Region

For some attributable vector  $\mathfrak{X}$ , we can take different values of range and range-rate  $(\rho, \dot{\rho})$  to complete the topocentric coordinates of the particle and thus obtain different physical orbits. Visually, we can imagine taking different points in the topocentric range / range-rate plane. However, not all of these orbits are relevant for any given application. Rather, a closed region of the  $(\rho, \dot{\rho})$  plane can be defined such that all of the physically relevant orbits are contained within the interior of this region. We define this region as the *admissible region*, and each discretized point on the admissible region as *virtual debris particles* (VD's). A set of criteria  $\mathcal{C}$  defining the admissible region has been proposed by Tommei, et al, and later refined by Maruskin, et al. [3] [6]. This set assumes radar observations for objects in low and medium Earth orbits (LEO, MEO):

$$\mathcal{C} = \bigcap_{i=1}^4 \mathcal{C}_i \quad (3)$$

and

$$\begin{aligned} \mathcal{C}_1 &= \{(\rho, \dot{\rho}) : E \leq 0\} & \mathcal{C}_2 &= \{(\rho, \dot{\rho}) : \rho_{\min} \leq \rho \leq \rho_{\max}\} \\ \mathcal{C}_3 &= \{(\rho, \dot{\rho}) : 1.03 \leq r_p\} & \mathcal{C}_4 &= \{(\rho, \dot{\rho}) : r_a \leq 25\}, \end{aligned} \quad (4)$$

where  $E$  is the specific geocentric energy of the debris particle,  $\rho_{\min}$  and  $\rho_{\max}$  are bounds for the physical range of the particle chosen “a priori,” and  $r_a$  and  $r_p$  are the apoapsis and periapsis radii of the orbit in units of Earth radii, respectively. In this paper, we set  $(\rho_{\min}, \rho_{\max}) = (0.3, 20)$  Earth radii as we are interested in all objects observable by optical sensors but outside of the range of radar sensors, corresponding to an altitude of 2000 kilometers (0.3 Earth radii) to 130,000 kilometers (20 Earth radii). Fig. 1 is an example of an admissible region.

## 2.3 Transformation of VD's

Let us consider the transformation of VD's from topocentric spherical coordinates (i.e.  $\alpha, \delta, \dot{\alpha}, \dot{\delta}, \rho, \dot{\rho}$ ) into Poincaré variables. Poincaré variables are the non-singular canonical counterpart to the equinoctial orbit elements [7]. Their main advantage is that the variables can be naturally grouped into coordinate-momenta symplectic pairs. Furthermore, they are defined and nonsingular even for circular and zero-inclination orbits. The Poincaré elements with respect to the classical orbit elements are given as:

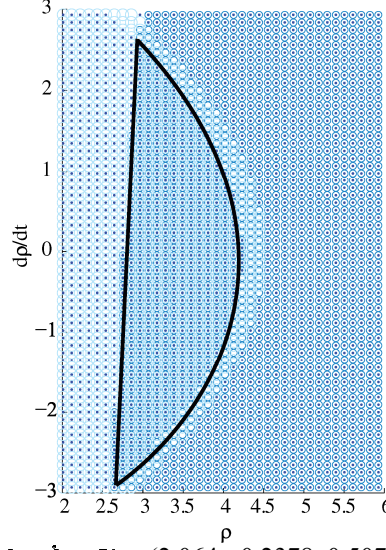


Fig. 1. An admissible region for  $\mathbf{x} = (\alpha, \delta, \alpha, \delta, \phi, \Theta) = (2.064, -0.2378, 0.5072, 0.0654, 0.1, 4.8)$ . The different shadings represent the different regions which satisfy each criterion in set  $\mathbf{C}$ ; thus, the admissible region is where all types of shading overlap, or the region outlined by the black line.

$$\begin{aligned}
 l &= \Omega + \omega + M & \mathfrak{L} &= \sqrt{\mu a} \\
 g &= \sqrt{2\mathfrak{L}(1 - \sqrt{1 - e^2})} \cos(\omega + \Omega) & \mathfrak{G} &= -g \tan(\omega + \Omega) \\
 \mathfrak{h} &= \sqrt{2\mathfrak{L}\sqrt{1 - e^2}(1 - \cos i)} \cos \Omega & \mathfrak{H} &= -\mathfrak{h} \tan \Omega,
 \end{aligned} \tag{5}$$

A detailed discussion is given in Fujimoto and Scheeres [8].

#### 2.4 The Geometry of Admissible Region Maps

Since the transformation from topocentric range / range-rate to Poincaré element space is one-to-one and invertible, the map of the admissible region is a 2-dimensional bounded submanifold, or a disk, in 6-dimensional Poincaré space [3] [8]. Suppose we have maps from two observations which have been dynamically evolved or regressed to a common epoch  $\tau$ :  $F^{\tau}_{\mathbf{x}_1}$  and  $F^{\tau}_{\mathbf{x}_2}$ . From the theory of general position, the dimension of intersection  $d$  between a pair of disks of dimension  $k$  and  $l$  in  $n$ -dimensional space is given as:

$$d = (k + l) - n, \tag{6}$$

where if  $d < 0$ , the two disks do not intersect randomly [2]. For our problem,  $d = (2 + 2) - 6 = -2$ , so if two admissible region maps intersect at all, it is extremely unlikely that they are two separate objects. In addition, equation (6) indicates that if we are to embed these disks in 5-dimensional Poincaré space such as the  $(\mathfrak{L}, \mathfrak{G}, g, \mathfrak{H}, \mathfrak{h})$  space, they will still not intersect randomly. Similarly, for 4-dimensional Poincaré space they intersect at a point, for 3-dimensions a line, and for 2-dimensions an area.

### 3. THE CORRELATION OF OBSERVATIONS AND PROBABILITY DISTRIBUTIONS

In this section, we outline how to use probability density functions of multiple data sets that characterize the debris population and combine them in some standard comparison space. Usually, this comparison space is the Poincaré element space described in Section 2.3 or some space derived from it. A direct application of this process is determining whether a number of observations are of the same object, and if they are, what the approximate orbital characteristics are.

Ultimately, we would like to know the probability of an optically observed object, characterized by attributable vector  $\mathbf{x}$ , being in the vicinity of some coordinate  $\mathbf{X}$  in a standard comparison space such as the Poincaré orbit

element space. This probability can be calculated for various values of  $\mathbf{X}$  across the comparison space, so it is beneficial to think of it as an element of a probability distribution function (pdf). We cannot rationally determine to any level of useful accuracy, however, neither this probability nor its distribution based on one optical observation, since  $\mathfrak{X}$  only contains 4 variables ( $\alpha, \delta, \dot{\alpha}, \dot{\delta}$ ) regarding the observed object's position and velocity, whereas 6 are required to fully describe the object's orbit. Therefore, it is necessary to combine multiple observations of the object. Here we face another problem. In a real-world setting, there is no guarantee that two or any number of arbitrary observations are of the same object; that is, that they are *correlated*. We would then like to know if some incoming data, such as a new observation, is related with the aforementioned pdf, and if so, how it affects the pdf.

In this paper, we consider the following data sets regarding Earth-orbiting objects and their observations:

**Set  $S_1$ :** Past observation data and debris distribution models. The United States Air Force Space Command (AFSPC) compiles and publicly distributes Two Line Element sets (TLEs) for all known objects that are in Earth orbit [1] [5]. Currently, the catalog consists of approximately 14,000 objects. Fig. 2 shows a scatter plot of the objects in orbit over  $a-e$  and  $a-i$  space.

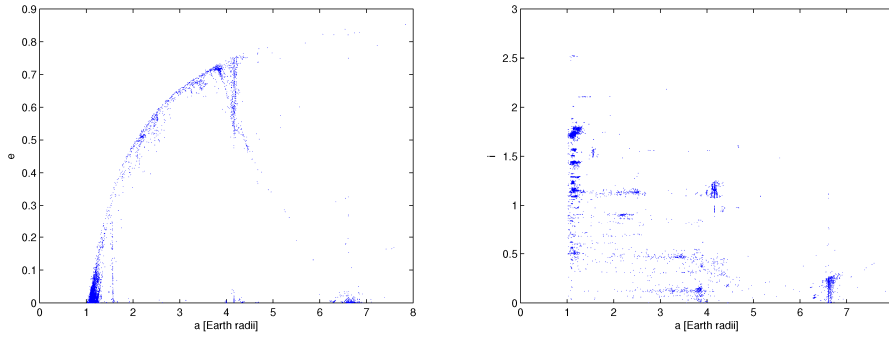


Fig. 2. Distribution of known objects in Earth orbit over  $a-e$  (left) and  $a-i$  (right) space.

Debris models incorporate computer simulations to account for objects too small to be observed (generally smaller than 1 meter for optical observations). MASTER-2005 by ESA is an example of such a model. The data in this category are discrete, and are independent of  $\mathfrak{X}$ .

**Set  $S_2(\mathfrak{X})$ :** The distribution of virtual debris (VD) particles over the standard comparison space. Although VD's are, by definition, uniformly distributed in the admissible region (i.e. range / range-rate space), for common choices for the comparison space such as orbit element and Poincaré space, the distribution of VD's in such spaces is non-uniform due to the non-linearity of the mapping. As a consequence, certain values of  $\mathbf{X}$  become more likely than others. The data in this category are continuous, and are a function of  $\mathfrak{X}$ . Computationally, however, a large and discrete sample set ( $\mathfrak{S}_2$ ) is used instead.

We discretize the standard comparison space into  $M (= \prod_{j=1}^6 M_j)$  6-dimensional hypercubes (or “bins”), which we index with vector  $\mathbf{i}$ . By doing so, we rationally group TLE objects, modeled debris, and VD's with similar orbital characteristics. In the comparison space, objects in a particular bin are spatially indistinguishable; i.e. we treat their coordinates as being the same as those that define the position of the bin. The discretization makes up for deficiencies in  $S_1$  data and undersampling of  $\mathfrak{S}_2$ , as well as speed up computational turnaround. Note that  $M$  is an important parameter, as if it is too small, we lose too much of the spacial resolution of the data sets. If  $M$  is too large, then the aforementioned data deficiencies and undersampling can negatively influence our results.

With this discretization, it is natural to consider the data in sets  $S_1$  and  $S_2$  as discrete pdf's spanning the comparison space rather than a set of countable elements. We refer to these pdf's as  $s_1(\mathbf{i})$  and  $s_2(\mathbf{i}, \mathfrak{X})$ , respectively. Practical definitions for  $s_1$  and  $s_2$  are given by first defining the following sets:

$$\begin{aligned} A_1 &= \{a : a \in S_1 \text{ and is mapped to bin } \mathbf{i}\} \\ \tilde{B}_1(\mathfrak{X}) &= \{\tilde{b} : \tilde{b} \in \mathfrak{S}_2(\mathfrak{X}) \text{ and is mapped to bin } \mathbf{i}\}. \end{aligned} \tag{7}$$

Then,

$$\begin{aligned} s_1(\mathbf{i}) &= \frac{n(A_i)}{n(S_1)} \\ s_2(\mathbf{i}, \mathbf{x}) &= \frac{n(\tilde{B}_i(\mathbf{x}))}{n(\tilde{S}_2(\mathbf{x}))}, \end{aligned} \quad (8)$$

where  $n(A_i)$  is the number of elements in set  $A_i$  and so on.

Suppose we have some prior discrete pdf  $g_{\mathcal{O}}(\mathbf{i}, \tau)$  that describes the probability that a particular object of interest  $\mathcal{O}$  is consistent with bin  $\mathbf{i}$  at epoch  $\tau$ . That is, if  $P$  is a probability measure and  $E_{\mathcal{O}}(\mathbf{i}, \tau)$  is an event where  $\mathcal{O}$  is consistent with  $\mathbf{i}$  at time  $\tau$ , then:

$$P[E_{\mathcal{O}}(\mathbf{i}, \tau)] = g_{\mathcal{O}}(\mathbf{i}, \tau). \quad (9)$$

$g$  can originate from the TLE catalog or a debris distribution model ( $S_1$ ), one observation or a set of observations that we believe are correlated *a priori* with  $\mathcal{O}$  ( $S_2$ ), or any combination of  $S_1$  and  $S_2$ . Here, we treat  $\mathbf{i}$  as a random variable that spans the bin index space. Also, all information has been propagated to  $\tau$ .

Now, let us consider a new series of information  $\{r\}$  that has come in from  $S_1$  or  $S_2$ , such as uncorrelated observations. We would like to calculate a posterior pdf  $h_{\mathcal{O}}(\mathbf{i}, \tau)$  on whether  $\mathcal{O}$  is consistent with bin  $\mathbf{i}$  and is related to  $\{r\}$ . It is obvious that  $h_{\mathcal{O}}(\mathbf{i}, \tau) = 0$  if the new information does not regard  $\mathcal{O}$ . In order to filter out such trivial cases, we let event  $\mathbf{x}_r^{\mathcal{O}}$  be one where the series  $\{r\}$  is related with  $\mathcal{O}$  and add this event as a condition to  $h$ . Using Bayes' theorem:

$$P[E_{\mathcal{O}}(\mathbf{i}, \tau) | \mathbf{x}_r^{\mathcal{O}}] = h_{\mathcal{O}}(\mathbf{i}, \tau) = \frac{f_{\{r\}}(\mathbf{i}, \tau) g_{\mathcal{O}}(\mathbf{i}, \tau)}{\sum_{\mathbf{j}} f_{\{r\}}(\mathbf{j}, \tau) g_{\mathcal{O}}(\mathbf{j}, \tau)}, \quad (10)$$

where the sum in the denominator is over all bins, and  $f_{\{r\}}(\mathbf{i}, \tau)$  is a pdf that describes the probability that  $\{r\}$  is consistent with bin  $\mathbf{i}$ :

$$P[E_{\{r\}}(\mathbf{i}, \tau)] = f_{\{r\}}(\mathbf{i}, \tau). \quad (11)$$

$E_{\{r\}}(\mathbf{i}, \tau)$  is an event where  $\{r\}$  is consistent with  $\mathbf{i}$  assuming all information has been dynamically evolved to  $\tau$ . Again,  $\mathbf{i}$  is treated as a random variable. If the information in  $\{r\}$  are observations,  $f$  is the admissible region of that observation mapped to the comparison space and to epoch  $\tau$ :  $f = s_2(\mathbf{i}, \mathbf{x})$ . Similarly, if the information is the TLE set, then  $f = s_1(\mathbf{i})$ . Note that from (6), if  $f > 0$  and  $g > 0$  at some bin  $\mathbf{i}$  regardless of discretization size, then  $\{r\}$  and  $\mathcal{O}$  are most likely related. Therefore, given  $\mathcal{O}$  is consistent with  $\mathbf{i}$ , whether  $\{r\}$  and  $\mathcal{O}$  are related depends only on whether  $\{r\}$  is consistent with  $\mathbf{i}$ :

$$P[\mathbf{x}_r^{\mathcal{O}} | E_{\mathcal{O}}(\mathbf{i}, \tau)] = f_{\{r\}}(\mathbf{i}, \tau). \quad (12)$$

Furthermore, the converse of the above argument ensures that as long as  $\{r\}$  and  $\mathcal{O}$  are related, then  $\sum_{\mathbf{j}} f \cdot g > 0$ , so (10) is well-defined.

In a graphical sense, pdf  $h$  is a "cut out" of the region where  $f$  and  $g$  intersect;  $h > 0$  for any bins where both  $f > 0$  and  $g > 0$ , and the probability expressed by  $h$  is one that is evaluated over this overlap region. Based on (6), we can look at whether  $h > 0$  for some bin  $\mathbf{i}$  to deduce with confidence whether or not the new information is related to the object of interest.

#### 4. NUMERICAL SIMULATIONS

In this section, we discuss results from an implementation of our method in MATLAB. Note that our goal is to show that our method is able to correlate objects and give an initial orbit estimate by giving it only angle and angle-rate information from the observations. Determining its robustness in real-world situations is future work.

We extracted 8 objects from the two-line element (TLE) catalog to obtain a sample set, and refer to them as follows [1]:

- 3 objects in GEO (GEO1~3),
- 1 object in a Molniya orbit (MOL1),
- 2 object in an eccentric MEO orbit (EM1,EM2),
- 1 object in a circular MEO orbit (CM1), and
- 1 GPS satellite (GPS1).

The orbital parameters of each object is given in Appendix A.

We simulated 996 zero-error observations of right ascension, declination, and their time derivatives made from 4 observatories for all 8 objects over the course of 24 hours. Thus,  $\mathbf{x} = (\alpha, \delta, \dot{\alpha}, \dot{\delta}, t_0, \Theta, \phi)$ , where  $t_0$  is the observation epoch and  $(\Theta, \phi)$  is the inertial angular position of the observation point. We can assume zero-error in the observations because the uncertainty in the angular information is generally much less than the uncertainty in the range and range-rate; refer to Fujimoto and Scheeres for a discussion on the effects of observation error to the outcome of our method [8]. The 4 observations points were located at:

- Socorro, New Mexico (33.8172°N 106.6599°W)
- Maui, Hawaii (20.7088°N 156.2578°W)
- Diego Garcia, British Indian Ocean Territory (7.41173°S 72.45222°E)
- Morón Air Base, Spain (37.170°N 5.609°W)

Approximately every 15 minutes, the code generates attributable vectors (i.e. simulated observations) for all objects that are above the local horizon at any given observation point.

We assumed no *a priori* information regarding the observed objects, and thus used a uniform initial pdf. The discretization of the Poincaré space was such that:

$$\mathbf{x}_{min} = \begin{bmatrix} 4.4621 \\ 0 \\ -5.0241 \\ -5.0241 \\ -5.0241 \\ -5.0241 \end{bmatrix}, \mathbf{x}_{max} = \begin{bmatrix} 12.6206 \\ 6.2832 \\ 5.0241 \\ 5.0241 \\ 5.0241 \\ 5.0241 \end{bmatrix} \quad (13)$$

and (100,77,123,123,123,123) bins in each coordinate direction for a total of  $1.7624 \times 10^{12}$  bins. All dynamics were two-body.

Fig. 3 is a graphical representation of the process explained in Section 3 for 2 observations. The red and green regions each represent pdf's based on observations that have been dynamically evolved to a common epoch (i.e. pdf's  $f$  and  $g$ ). The propagation has "shredded" the red pdf in the  $\mathcal{Q}$ - $\mathcal{I}$  plane [3]. The blue region is the combined distribution (i.e. pdf  $h$ ). The yellow asterisk is the true state of the observed object. The distributions have been projected onto 2-dimensional subspaces using their coordinate-conjugate momentum pairs; note, however, that the correlation was conducted in the full 6-dimensional Poicaré space. When correlating two observations of the same object (top), we see that  $h > 0$  for a very small region of the state space; for this particular example,  $h > 0$  for 11 bins. Furthermore, the true state is included in the region in state space where  $h > 0$ . Therefore, the state estimate is good. On the other hand, when two observations are of different objects (bottom),  $h = 0$  for the entire state space, which allows us to conclude that the two observations are unrelated.

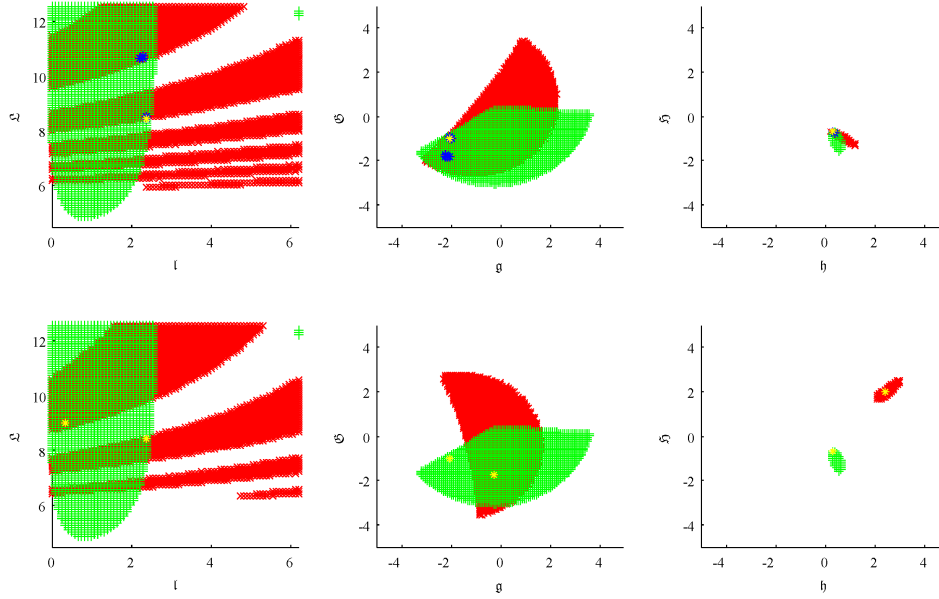


Fig. 3. Projections of probability distributions when correlating observations of the same object (top; EM1-EM1) and a different object (bottom; EM1-EM2). Length units in Earth radii, time units in hours, mass units in kilograms, angle units in radians.

Our correlation process performed well for all 996 observations: all observations were correctly correlated to the 8 objects and their states were correctly estimated down to a region of at most 4 bins. Thus, there were no “false positive” results. We developed a linearization technique in which the pdf’s are mapped linearly, reducing the computational time while attaining good accuracy [8]. On a dual-core Xeon server with 32-bit numerics, each correlation run took approximately 10 minutes. If we wish to further reduce the region over  $h > 0$  as well as reduce computation time, we can assume *a priori* that all observed objects were included in either the TLE catalog or some debris distribution model instead of the uniform distribution assumption we made for Fig. 3. Then, the admissible region maps are “pre-conditioned” to exclude unrealistic objects. Correlation times were reduced to 1 to 2 minutes. Table 1 lists the number of overlap bins for each correlated object.

{r}	Uniform		Preconditioned	
	Overlap bins	Contains true state	Overlap bins	Contains true state
GEO1	4	YES	2	YES
GEO2	3	YES	2	YES
GEO3	4	YES	2	YES
MOL1	1	YES	1	YES
EM1	2	YES	1	YES
EM2	3	YES	1	YES
CM1	2	YES	1	YES
GPS1	3	YES	1	YES

Table 1. The estimation accuracy of each observed object when using a uniform initial pdf (left) and the TLE as the initial pdf (right).

## 5. LIMITING CASES

In this section, we investigate special observations cases where we expect the method to have difficulty in calculating an accurate initial orbit estimate; namely, when two objects lie within a bin size, when an object is observed simultaneously at two observation points, and when objects in a satellite constellation are observed over long periods of time.

### 5.1 Limitation of Bin Resolution

Recall from Section 3 that all objects within a bin are regarded as having the same state parameters. Therefore, there may be cases where two satellites that are close in state space are falsely correlated. We can always overcome this limitation by increasing the fidelity of the discretization; one efficient way is to implement a recursive algorithm where the bin size is decreased in the vicinity of overlapping region. Moreover, we can be smart about how we initially discretize the space. For instance, we expect that a finer grid is necessary in the  $\mathbf{l}$  direction (i.e. mean anomaly) compared to the  $\mathbf{g}$  direction (i.e. semi-major axis).

### 5.2 Simultaneous Observations of an Object

The proposed method may run into difficulties computing a precise state estimate when the two pdf's are near parallel. Although such pdf's would still most likely intersect at a single point, they may appear to occupy the same bins in the discretized state space (i.e. overlap) over a large region. One case where pdf's become near parallel is when an object is observed simultaneously at 2 different observations points, as seen in Fig. 4. Here, pdf  $h$  spans over 688 bins using the nominal discretization in Section 4. This result, however, does not imply that the two pdf's intersect over a large planar region; from (6), 2-dimensional intersections of pdf's are extremely unlikely. Indeed, as we refine the discretization by 20%, then 50%, the overlap region begins to converge upon the coordinate of the true object state. Note that compared to the method proposed by Maruskin, et al. which evaluates intersections of manifolds within their 2-dimensional projections, the new method converges faster as the intersections are evaluated in the full 6-dimensional space [3].

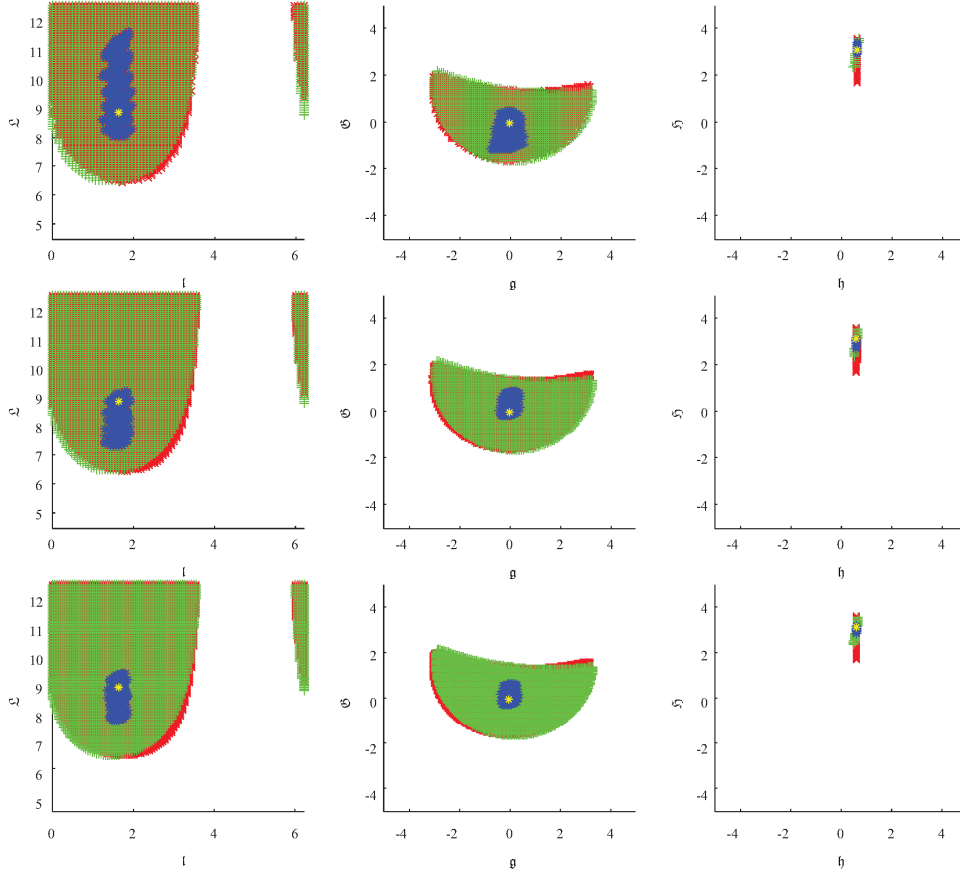


Fig. 4. Combined pdf  $h$  of two near-parallel pdf's (CM1 observed simultaneously at  $(\Theta, \varphi) = (1, 1)$  and  $(1.5, 2)$  at time  $t = 26.36$  hours) as the discretization is refined from  $M = 1.7624 \times 10^{12}$  (top) to  $1.2M$  (middle) and  $1.5M$  (bottom).

### 5.3 Observations of Satellite Constellations

Suppose we make two observations separated by, say, 4 hours, which are consistent to the same orbit plane. We can either conclude that we observed 1 object with an orbital period that is any divisor of 4, or that we observed 2 different objects in a satellite constellation with an orbit period that is any divisor or multiple of 4. For this particular example, most of the solutions in the former set will have a semi-major axes that are too small to be included in the admissible region. If the temporal separation of the observations were larger, however, then single-object solutions may become viable. The long-term propagation “dilutes” information regarding the object’s angular position that we can extract from the observation separation time.

Mathematically, let two object be on an orbit with period  $\tau$  separated by mean anomaly  $\Delta M$ . In two-body motion,  $\tau$  is related to semi-major axis as  $\tau = 2\pi\sqrt{a^3/\mu}$ . Suppose we observe one of the objects at time 0, and then the other at time  $N\tau + (\Delta M/n)$ , where  $N \in \mathbf{N}$  and  $n$  is the mean motion; i.e. we observe the second object after  $N$  revolutions. Now, if we were to wrongly assume that we observed the same object twice, then the true anomaly  $a + \Delta a$  of this fictitious object is:

$$\begin{aligned} 2\pi N \sqrt{\frac{a^3}{\mu}} + \frac{\Delta M}{n} &= 2\pi N \sqrt{\frac{(a + \Delta a)^3}{\mu}} \\ \Leftrightarrow \frac{\Delta a}{a} &= \left(1 + \frac{\Delta M}{2\pi N}\right)^{2/3} - 1. \end{aligned} \quad (14)$$

Therefore,  $N \rightarrow \infty \Rightarrow \Delta a/a \rightarrow 0$ . If the first observation generated a non-empty admissible region, then it is likely that the proposed method will mistakenly relate the two observations given they are temporally well-separated.

Fig. 5 is a graphical representation of the above scenario. We simulated observing 2 separate objects in a constellation from one observatory with different observation separation times. When the separation is 14.85 hours, the combined pdf is null at all bins, meaning the method successfully recognizes the observations as that of different objects. When the separation is increased to 60.61 hours, however, we see that the 2 pdf’s overlap, and thus we obtain a “false positive” result.

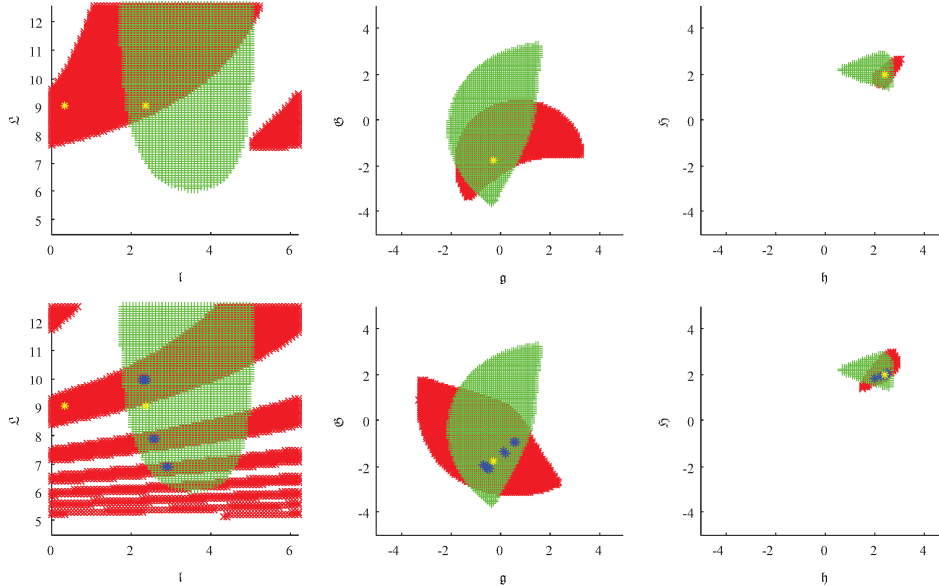


Fig. 5. Correlation of observations of 2 different objects separated by a mean anomaly of  $2/3\pi$  on the same orbital plane as EM2. Observations are separated by 14.85 hours (top) and 60.61 hours (bottom). All observations are made at  $(\Theta, \varphi) = (2, 4)$ .

## 6. CONCLUSIONS

In this paper, we discussed methods of correlating multiple optical observations as well as providing initial state estimates using pdf's in the Poincaré orbit element space. We outlined the method that incorporates Bayes' rule. An implementation of the method in MATLAB successfully correlated 996 optical observations and provided good initial orbit estimates. Finally, some limiting cases were examined.

Future work will be incorporate more accurate dynamics, and to apply our method to different observation scenarios such as space-based observations and observations of objects in heliocentric orbit.

## 7. APPENDIX A: ORBITAL ELEMENTS FOR OBJECTS IN THE NUMERICAL EXAMPLE

The classical and Poincaré orbital elements of all 8 objects in our simulation sample set are listed below as:

$$(\alpha [r_E], e, i [\text{rad}], \Omega [\text{rad}], \omega [\text{rad}], M [\text{rad}], (\mathcal{Q} [r_E^2/\text{hour}], l [\text{rad}], \mathcal{G} [r_E/\text{hour}^{1/2}], g [r_E/\text{hour}^{1/2}], \mathcal{S} [r_E/\text{hour}^{1/2}], h [r_E/\text{hour}^{1/2}]),$$

where  $r_E$  is Earth radius.

- GEO

**GEO1** (6.6102,0.0003,0.0002,3.1274,2.3294,5.7226) (11.4721,4.8962,0.0006,0.0006,-0.0000,-0.0006)

**GEO2** (6.6109,0.0003,0.0009,5.9501,2.9681,5.8729) (11.4727,2.2247,-0.0005,-0.0009,0.0010,0.0029)

**GEO3** (6.6109,0.0001,0.0001,3.0902,4.2464,6.1176) (11.4727, 0.8879,-0.0003,0.0001,-0.0000,-0.0002)

- Molniya

**MOL1** (4.1971,0.7154,1.1204,0.8126,5.1137,0.1671) (9.1414,6.0934,0.8200,2.1991,-1.9501,1.8469)

- Eccentric MEO

**EM1** (3.6573,0.7123,0.3106,1.0976,1.6080,5.9942) (8.5333, 2.4166,-0.9526,-2.0447,-0.6739,0.3451)

**EM2** (4.1472,0.5529,1.2347,5.5811,2.4137,4.8996) (9.0868,0.3281,-1.7237,-0.2444,2.0573,2.4323)

- Circular MEO

**CM1** (3.9994,0.0006,1.1284,4.9148,4.2128,2.9461) (8.9234,5.7905,-0.0005,-0.0017,3.1297,0.6421)

- GPS satellite

**GPS1** (4.1645,0.0048,0.9599,2.7242,3.6934,2.5851) (9.1057,2.7195,-0.0019,0.0143,-1.1296,-2.5474)

## 8. REFERENCES

1. Satellite situation report. Report, HQ AFSPC/XOCS.
2. J. S. Carter. *How Surfaces Intersect in Space: An introduction to topology*. World Scientific, Singapore, second edition, 1995.
3. J. M. Maruskin, D. J. Scheeres, and K. T. Alfriend. Correlation of optical observations of objects in earth orbit. *Journal of Guidance, Control and Dynamics*, 32(1):194–209, 2009.
4. A. Milani, G. Gronchi, M. Vitturi, and Z. Knežević. Orbit determination with very short arcs. i admissible regions. *Celestial Mechanics and Dynamical Astronomy*, 90:57–85, 2004.
5. A. Rossi. The earth orbiting space debris. *Serb. Astron. J.*, (170):1–12, 2005.
6. G. Tommei, A. Milani, and A. Rossi. Orbit determination of space debris: admissible regions. *Celestial Mechanics and Dynamical Astronomy*, 97:289–304, 2007.
7. D. Vallado. *Fundamentals of Astrodynamics and Applications*. Microcosm Press, Hawthorne, CA, third edition, 2007.
8. K. Fujimoto, and D. J. Scheeres. Correlation of Optical Observations of Earth-Orbiting Objects by Means of Probability Distributions. Presented at the *2010 AIAA/AAS Astrodynamics Specialist Conference*, AIAA-2010-7975.